Path integral Monte Carlo simulations of dense carbon-hydrogen plasmas

Shuai Zhang,[1,2,a)] Burkhard Militzer,[1,3,b)] Lorin X. Benedict,[2] François Soubiran,[1] Kevin P. Driver,[1,2] and Philip A. Sterne[2]

[1)] *Department of Earth and Planetary Science, University of California, Berkeley, California 94720, USA*
[2)] *Lawrence Livermore National Laboratory, Livermore, California 94550, USA*
[3)] *Department of Astronomy, University of California, Berkeley, California 94720, USA*

Carbon-hydrogen plasmas and hydrocarbon materials are of broad interest to laser shock experimentalists, high energy density physicists, and astrophysicists. Accurate equations of state (EOS) of hydrocarbons are valuable for various studies from inertial confinement fusion (ICF) to planetary science. By combining path integral Monte Carlo (PIMC) results at high temperatures and density functional theory molecular dynamics (DFT-MD) results at lower temperatures, we compute the EOS for hydrocarbons from simulations performed at 1184 separate (ρ, T)-points distributed over a range of compositions. These methods accurately treat electronic excitation and many-body interaction effects, with no adjustable parameters or experimental input. PIMC is also an accurate method that is capable of treating nuclear quantum effects at finite temperatures. These methods therefore provide a benchmark-quality EOS that surpasses that of semi-empirical and Thomas-Fermi-based methods in the warm dense matter regime. By comparing our first-principles EOS to the LEOS 5112 model for CH, we validate the specific heat assumptions in this model but suggest that the Grüneisen parameter is too large at low temperature. Based on our first-principles EOS, we predict the principal Hugoniot curve of polystyrene to be $\sim 5\%$ stiffer at maximum shock compression than that predicted by orbital-free DFT and other Thomas-Fermi-based approaches. By investigating the atomic structure and chemical bonding of hydrocarbons, we show a drastic decrease in the lifetime of chemical bonds in the pressure interval from 0.4 to 4 megabar. We find the assumption of linear mixing to be valid for describing the EOS and the shock Hugoniot curve of hydrocarbons in the regime of partially ionized atomic liquids. We make predictions of the shock compression of glow-discharge polymers and investigate the effects of oxygen content and C:H ratio on its Hugoniot curve. Our full suite of first-principles simulation results may be used to benchmark future theoretical investigations pertaining to hydrocarbon EOS, and should be helpful in guiding the design of future experiments on hydrocarbons in the gigabar regime.

I. INTRODUCTION

Accurate equations of state (EOS) of materials under various temperature and pressure conditions is of fundamental importance in earth and planetary science, astrophysics, and high energy density physics.[1] These applications require that we understand matter that is partially ionized and strongly coupled. This includes conventional condensed matter ($T \ll T_{\text{Fermi}}$), warm dense matter ($T \sim T_{\text{Fermi}}$), and weakly coupled plasmas ($T \gg T_{\text{Fermi}}$ and $\langle$potential energy$\rangle \ll \langle$kinetic energy$\rangle$). At high temperatures ($>10^2$ eV) and near-ambient densities, electrons and nuclei can generally both be treated as ideal gases, due to complete ionization of atoms into a perfect plasma state. At slightly lower temperatures, the Debye-Hückel model may be used to treat weak interactions within a screening approximation. Materials in condensed forms are characterized by both strong coupling and degeneracy effects and thus require sophisticated quantum many-body methods for their description. However, very good progress can be made with average-

atom methods such as average-atom Thomas-Fermi theory and average-atom Kohn-Sham Density Functional Theory (DFT), in which isolated ions are embedded within a spherically-symmetric electron liquid. Kohn-Sham-DFT average-atom methods resolve distinct electronic shells of atoms, just as in conventional applications of quantum theory to isolated atoms, but they do not account for directional bonding between atoms and therefore fail at low temperatures. Thomas-Fermi and more general orbital-free (OF) DFT approaches do not account for electronic shell effects and are thus unable to properly describe partially ionized plasmas; as such, they provide a less than satisfactory description of warm dense matter.

EOS models (e.g., of the QEOS type[2]) treating wide ranges of density and temperature and databases that house them (e.g., SESAME[3] and LEOS), make heavy use of average-atom theories for electronic excitations, *ad hoc* interpolation formulas which mediate the evolution of the ionic specific heat from low-T to the high-T ideal gas limit, and semi-empirical models which allow for the fitting of experimental results near ambient conditions. The efficacy of these EOS models is questionable precisely in the regimes currently probed in dynamic compression experiments reaching gigabar (Gbar) pressures, in which it is expected that atoms are significantly (though not fully)

ionized by both temperature and pressure. Clearly, this regime is in need of more sophisticated theoretical treatments which more fully account for detailed electronic structure and many-body effects.

First-principles molecular dynamics (MD) based on DFT is widely used for calculating the atomic structure, the EOS, and other electronic and ionic properties of materials at relatively low temperatures, where the ionization fraction is small. In DFT-MD, the nuclei are usually treated as classical particles whose motion follows Newton's equation of motion, whereas the potential field is determined by solving a single-particle mean-field equation self-consistently using DFT. This method naturally includes the anharmonic terms of nuclear vibrations and is usually a good approximation for systems with heavy elements, and is widely used for simulations of earth and planetary materials[4–9]. For light elements, zero-point motion cannot be neglected[10,11], which makes important contributions to the energy that may alter relative phase stability. At temperatures above 100 eV, DFT-MD of the Kohn-Sham variety becomes computationally intractable due to the considerable number of high-lying single-electron states that need to be included. It is also practically limited by the use of pseudopotentials that reduce computational costs by freezing inner-shell electrons within ionic cores that tend to overlap between neighboring atoms if the system is at significant compression, leading to errors.

Path integral Monte Carlo (PIMC)[12,13] offers an approach to directly solve the many-body Schrödinger equation in a stochastic way. It typically treats nuclei and electrons as quantum paths that evolve in imaginary time, and obtains the energy and other properties of a system by solving for the thermal density matrix and computing thermodynamic averages within the sampled ensembles. For Fermionic systems, a suitable nodal structure is required to restrict the sampling space in order to solve the sign problem that arises from anti-symmetry of the many-body density matrix. Accuracy of the method has been established by early work on fully-ionized hydrogen[14,15] and helium[16] plasmas. In the past five years, developments by extending free-particle nodes[17] or implementing localized orbitals[18] to construct the nodes have enabled PIMC studies of a series of heavier elements and compounds[17–29]. These works have applied PIMC to EOS calculations at temperatures ranging from a few hundred million K to as low as 2.5×10^5 K. For first- and second-row elements, PIMC and DFT-MD simulations produce consistent EOS results at intermediate temperatures.

While computer simulations with classical nuclei provide sufficiently accurate predictions for a wide range thermodynamic conditions, at low temperature, nuclear quantum effects (NQEs) often play an important role in predicting observed phenomena[30]. One typically compares the interparticle spacing to the thermal de Broglie wavelength ($\sim 1/\sqrt{mk_{\mathrm{B}}T}$) that is inversely proportional to the square root of mass and temperature, and, there-

fore cold and low-Z materials are strongly influenced by NQE. Often such effects are referred to as zero point motion. In solids, zero point effects are typically studied with lattice dynamics calculations that derive the spectrum of vibrational eigenmodes within the quasi-harmonic approximation. Such calculations rely on the second derivative the energy with respect to the nuclear positions that can be derived with theoretical methods of various levels of accuracy ranging from classical force fields[31], DFT[32,33], and in principle also with quantum Monte Carlo calculations[34]. It is difficult, however, to introduce anharmonic effects accurately into the lattice dynamics approach[35]. Anharmonic effects are important for temperatures above the Debye temperature, in particular near melting, but also at very low temperature in materials that are rich in hydrogen or helium. Because of their small mass, the nuclear wavefunctions often spreads into the anharmonic regions of the confining potential even at the ground state so that anharmonic effects can no longer be neglected.

Path integral methods[36] can accurately incorporate NQE and anharmonic effects at all temperatures and can describe solids as well as liquids[37,38]. An efficient approach, that has been devised to pursue NQE problems, is to combine the path integral method for nuclei with other electronic structure methods, such as DFT or quantum Monte Carlo, to efficiently describe the forces between the nuclei. Path integral molecular dynamics[39] and coupled electron ion Monte Carlo[40] are two common techniques that employ this combined approach[41]. A few examples include phase transitions in solid[11,42] and liquid[10,43,44] hydrogen, helium[16,45], hydrogen-bonding in water[46–48], solid water-ice phases[49,50], phonon dispersion in diamond[51] and energy barriers for small molecules[52,53].

In this work, we employ the path integral methods to study partially and highly excited electrons. Even though the temperatures under consideration are quite high ($\sim$100 eV), fermionic effects are crucial to characterize the electronic states accurately. The occupation of bound electronic states affects the motion of the nuclei through Pauli exclusion. At high density, the motion of the nuclei deforms the shape of the electronic orbitals. Thus, a fully self-consistent approach is needed for materials in the WDM regime.

We apply PIMC simulations with free-particle nodes and DFT-MD calculations to study carbon-hydrogen compounds. Hydrocarbons are currently in use as ablator materials in dynamic compression and inertial confinement fusion (ICF) experiments[54–58]. Materials such as polystyrene and glow-discharge polymer (GDP) have been a strong point of interest and extensively studied by both theorists and experimentalists[59–81]. Recently, laser shock experiments at the National Ignition Facility (NIF)[82–87] and the OMEGA Laser facility[88] have extended the ablation pressure in CH to the Gbar range[89]. Calculations employing DFT-MD or OF-DFT have been performed to study the EOS of hydrocarbon materi-

als[79,90–96]. These theoretical studies predicted shock Hugoniot curves that agree well with experiments at low temperatures. At high temperatures, Kohn-Sham DFT is unfeasible while OF-DFT works efficiently but its predictions are yet to be tested by other theories[24] and experiments. We expect the PIMC and DFT-MD simulations of this study to produce predictions for the EOS of hydrocarbons which are sufficiently accurate to be used as benchmarks for both the construction of wide-range EOS models, and the further investigation of hydrocarbon EOS with less computationally expensive simulation methods. Ultimately, our predictions may prove useful for the design and interpretation of dynamic compression and ICF experiments in the future.

The paper is organized as follows: Section II introduces the details of our simulation methods. Sec. III presents our EOS results, the shock Hugoniot curves, and comparisons with other theories, models, and experiments. Sec. IV discusses the structural evolution of hydrocarbons and the shock compression of GDP and related materials. We conclude in Sec. V.

II. SIMULATION METHODS

We use the CUPID code[97] for our PIMC simulations within the fixed-node approximation[98]. We treat the nuclei as quantum particles, even though the kinetic energy is much larger than the zero-point contribution to the total energy of the system at the high temperatures ($T \geq 10^6$ K = 87 eV) considered here. Electrons are treated as fermions. Their quantum paths are periodic in the imaginary time interval, $0 \leq t \leq \beta = 1/k_\mathrm{B}T$ (k_B is the Boltzmann constant), but the paths of electrons with the same spin may be permuted as long as they do not violate the nodal restriction[98]. Following our previous work on hydrogen[14,15,38,99–104], helium[105,106], and carbon[17,19], we use free-particle nodes to constrain the sampling space by restricting the paths to positive regions of the density matrix of ideal fermions. Coulomb interactions between all pairs of particles are introduced via pair density matrices[107,108]. The pair density matrices are evaluated at an imaginary time interval of 1/1024 Hartree^{-1} (Ha^{-1}) while the nodal restriction is enforced in steps of 1/8192 Ha^{-1}.

For DFT-MD simulations, we use the Vienna *Ab initio* Simulation Package (VASP)[109]. We choose the hardest available projected augmented wave (PAW) pseudopotentials[110] with core radii of 1.1 and 0.8 Bohr for C and H, respectively. All electrons are treated as valence electrons. Exchange-correlation effects are treated within the local density approximation (LDA)[111,112]. We choose a large plane-wave basis cutoff of 2000 eV, the Γ point to sample the Brillouin zone, and an MD time step of 0.05-0.2 fs, depending on the temperature. MD trajectories are generated in an *NVT* ensemble, and typically consist 2000-10000 steps to make sure the system is in equilibrium and the energies and pressures are converged.
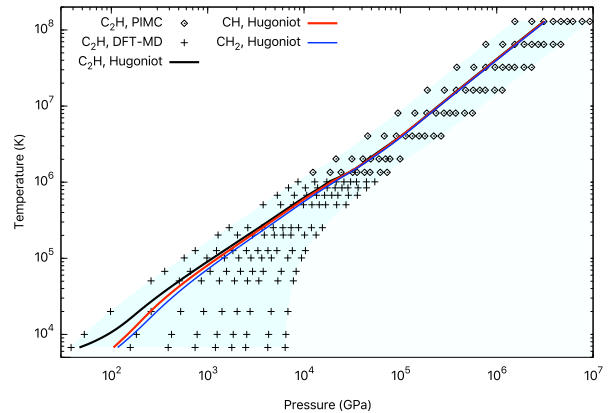

FIG. 1. Pressure-temperature conditions considered in our PIMC and DFT-MD simulations of hydrocarbons. For clarity, only the EOS data for C_2H and the Hugoniot curves of C_2H, CH, and CH_2 are shown. The Hugoniot curves are obtained by setting the initial density to 1.12, 1.05, and 0.946 g/cm^3 for C_2H, CH, and CH_2, respectively. The shaded region denotes the approximate area that the EOS of all hydrocarbons studied in this work fall in.

The temperature is controlled with a Nosé thermostat[113]. All VASP energies are shifted by -37.4243 Ha/C and -0.445893 Ha/H, to put DFT-MD energies on the same scale as those of PIMC. These values are determined by performing all-electron single-atom calculations using the OPIUM code[114].

We study six different compositions by simulating $C_{20}H_{10}$, $C_{18}H_{18}$, $C_{16}H_{24}$, $C_{14}H_{28}$, $C_{12}H_{36}$, and $C_{10}H_{40}$ in a cubic cell at temperatures between 10^6-1.3×10^8 K using PIMC and 2.5×10^5-10^6 K using DFT-MD. We use larger cells with four times as many atoms at the lower temperatures of 6.7×10^3-2.5×10^5 K in order to eliminate finite-size effects, which are expected to be larger at low temperatures[17]. In order to maximize the computational efficiency of the large-cell simulations, we freeze the $1s^2$ electrons of carbon in the pseudopotential core without losing accuracy, because the temperatures are much lower than the ionization energy (392 eV for $1s^2$ of C)[115]. We consider a grid of nine isochores for each hydrocarbon system, chosen so that the pressure ranges for each composition are similar; this results in densities for CH between (2 - 12)$\times\rho_\mathrm{ambient}$ (see Fig. 1). These conditions are both relevant to dynamic compression experiments, and well within the range in which Kohn-Sham DFT-MD simulations with pseudopotentials are feasible.

We also investigate the validity of the linear mixing approximation for estimating the EOS of various hydrogen-carbon mixtures. In this method, the energy and the density of the mixture are obtained with the isobaric, isothermal additive volume assumption via $V_\mathrm{mix}(P,T) = f_\mathrm{C}V_\mathrm{C}(P,T)+f_\mathrm{H}V_\mathrm{H}(P,T)$ and $E_\mathrm{mix}(P,T) = f_\mathrm{C}E_\mathrm{C}(P,T)+f_\mathrm{H}E_\mathrm{H}(P,T)$, where $f_\mathrm{C} = n_\mathrm{C}/(n_\mathrm{C}+n_\mathrm{H})$ and $f_\mathrm{H} = n_\mathrm{H}/(n_\mathrm{C}+n_\mathrm{H})$ are the mixing ratios, V_mix, V_C, V_H are volumes per atom for the mixture, pure carbon, and

pure hydrogen respectively (and likewise for the internal energies, E). $E(T, P)$ and $V(T, P)$ of the pure species are constructed using bi-variable spline fitting over the ρ-T space spanned by the EOS of pure hydrogen and pure carbon. The shock Hugoniot curves derived with simulations of the fully interacting system can be compared to that obtained with the linear mixing approximation.

III. RESULTS

A. Equation of state

Figure 2 shows the calculated EOS for C_2H along nine isochores. A complete list of EOS data for other hydrocarbons (C_2H_3, CH_2, CH_3, CH_4) in this study are in the supplementary material. Our simulation results for CH are available in Ref. 29. The internal energies and pressures from PIMC calculations agree with predictions of the Debye-Hückel model at temperatures above 4×10^6 K and with the Fermi electron gas theory (wherein both ions and electrons are treated as uniform-density free Fermi gases) above 8×10^6 K, which is higher than the $1s^1$ ionization energy (489.99 eV or 5.7×10^6 K)[115] of carbon. PIMC results show excellent agreement with DFT-MD at 10^6 K, with differences typically less than 1 Ha/carbon in internal energy and 3% in pressure. We have therefore constructed a consistent first-principles EOS table for warm dense hydrocarbons, over a wide density-temperature range of 1.4-13.5 g/cm^3 and 6.7×10^3-1.3×10^8 K and C:H=2:1-1:4. The good consistency of PIMC with DFT-MD and the other high-temperature theories validates the use of the free-particle nodes in PIMC for temperatures as low as 10^6 K, and PAW pseudopotentials and zero-temperature exchange-correlation functionals in DFT-MD up to 10^6 K.

In comparison with a recent first-principles study[94] that employs DFT-MD with the Perdew-Burke-Ernzerhof (PBE)[116] exchange-correlation functional at temperatures below T_{Fermi}, the P-T and E-T curves coincide with LDA curves in this work. This indicates the EOS does not significantly dependent on the form of the exchange-correlation functional in the temperature interval under consideration. At 10^6 K and higher temperatures, the energy of Ref. 94 is different from PIMC predictions of this work while the pressure differences are small. This is associated with underestimation of the compression maximum by OF-DFT that is used in Ref. 94. More details on this will be discussed in Sec. III C.

B. Comparisons with the LEOS-5112 model for CH

An important aim of this work is to produce benchmarking EOS predictions that will act as constraints in the future construction of EOS models for hydrocarbons which span wide ranges of density and temperature,
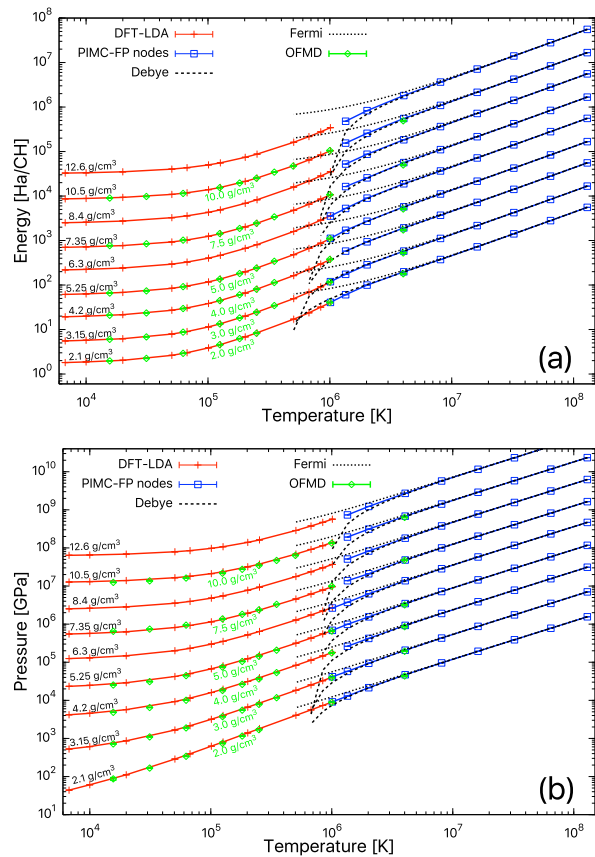

FIG. 2. Internal energies and pressures of CH along isochores. Corresponding results of the Fermi-gas and the Debye-Hückel theories are plotted for comparison. PIMC predicts consistent results with DFT-MD at 10^6 K PIMC and agrees with ideal Fermi gas and Debye-Hückel models at above 8×10^6 K. As temperature decreases, the ideal Fermi gas model significantly overestimates the energy and the pressure because of the neglect of interactions. Debye-Hückel model improves over the Fermi-gas model for temperatures down to 3×10^6 K but leads to low pressures and energies at lower temperatures, at which electron-nucleus coupling gets stronger and the screening approximation breaks down. DFT-MD and OF-DFT results from Ref. 94 are shown with green diamonds for comparison. Error bars of the data are much smaller than the size of the symbols. Different isochores have been shifted apart for clarity.

well beyond that where experimental data is available. It is therefore interesting to compare the details of *existing* EOS models for, e.g., CH to the first-principles predictions in this work. The most recent such model for polystyrene (CH) constructed at the Lawrence Livermore National Laboratory is LEOS-5112, closely related to LEOS-5400[117], currently used as the EOS model of choice for GDP in inertial confinement fusion simulations where that material is employed as an ablator. EOS models such as these assume that the free energy is decomposable into separate ionic and electronic excitation terms. While somewhat justified due to the large ion/electron
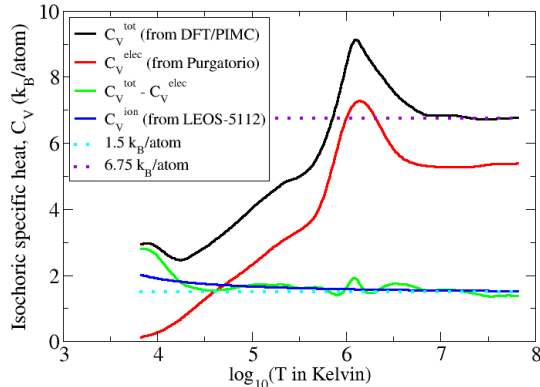
FIG. 3. C_V for CH at a density of $\rho = 3.15$ g/cm^3. The black curve is C_V as extracted from a spline fit of our discrete $E(T)$ predictions from first-principles simulations at this density. See the text for descriptions of the other curves.
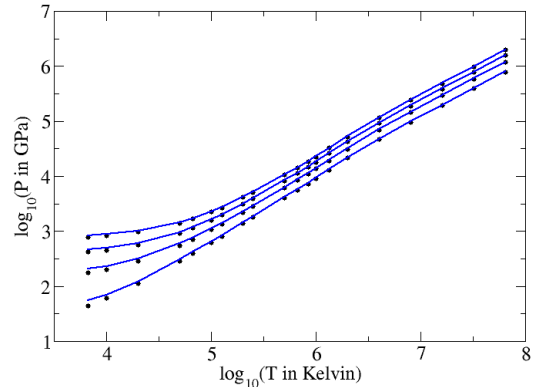

FIG. 4. Total pressure isochores for CH at densities $\rho = 2.1$, 3.15, 4.2, and 5.25 g/cm^3 (in the sequence of bottom to top). The black symbols are the results of our DFT-MD ($T \leq 10^6$ K) and PIMC ($T > 10^6$ K) simulations. The blue curves are the corresponding pressure isochores from LEOS-5112.

mass ratio, it is important whenever possible to compare to EOS predictions from *ab initio* methods (such as PIMC) that do *not* make this assumption.

The LEOS-5400 EOS model[117] was originally constructed to represent the non-stoichiometric carbon-hydrogen-oxygen composition of GDP, and to reproduce both Hugoniot and off-Hugoniot measurements (specifically, shock-and-release from an interface with deuterium)[81]. More recently, LEOS-5112 was developed to facilitate comparison with experiments and simulations on the stoichiometric material, CH. This CH model closely follows the parameters used to make GDP LEOS-5400.

The cold curve, $E(V, T = 0)$, was based on a constant-pressure mix of the corresponding Thomas-Fermi cold curves for pure C and pure H, with a bonding correction[2] to set the density at 1.049 g/cm^3 and the bulk modulus at 0.9 GPa at a temperature of 20 K. This relatively high bulk modulus was softened by using a break point[118] that changes the cold curve energy by $\delta E = Au^3/(B + u^3)$ for $u \geq 1$ where $u = \rho/\rho_0$, $A = -8$ kJ/g and $B = 3.0$. A corresponding change was also made to the cold curve pressure. The relatively high bulk modulus value, together with the break point, reproduces both the initial equilibrium conditions of the material (at cryogenic conditions), and the higher-temperature behavior above 50 GPa, which is higher than the graphite-diamond transition pressure along the Hugoniot ($\sim$15-25 GPa).

The terms in the free energy accounting for ionic excitations (ion-thermal) were modeled using both a Debye-Grüneisen model and a dissociation model. The Debye model used a Debye temperature of 650 K at equilibrium density and an ion-thermal Grüneisen γ at this point of 0.99. This value of γ was originally chosen to give the experimentally observed thermal expansion of GDP between 20 K and room temperature. The Grüneisen pa-

rameter was kept constant from ρ_0 up to a density of 2.7 g/cm^3, at which point it was gradually decreased to 0.81 at 10 g/cm^3 and 0.5 at very high density. For densities below 1.049 g/cm^3, the Grüneisen gamma reduces gradually to the ideal-gas value of 2/3. The variation in the Debye temperature is computed from this $\gamma(\rho)$ function[2]. The dissociation model adds an additional contribution to the free energy which models the dissociation of a dimer[118]. The main purpose of this term is to model chemical dissociation in a simplified way, as if it were due to diatomic molecular dissociation. In the GDP model, this extra flexibility allowed simultaneous fits to both Hugoniot data and off-Hugoniot release data. This same model was retained in LEOS-5112 without modification. The model includes a dimer dissociation energy of 0.7 eV and a nominal rotational temperature of 20 K.

The liquid contribution to the ion-thermal free energy in LEOS-5112 (and LEOS-5400) is given by a Cowan model[2] with an exponent of 1/3,

$$C_V^{\text{ion}} = \frac{3k_B}{2} + \frac{3k_B}{2}\left[\frac{T_m(\rho)}{T}\right]^{1/3} \tag{1}$$

This ensures that the ionic contribution to the specific heat decays from $3k_B$/ion to the ideal gas value of 1.5 k_B/ion as $T \to \infty$. $T_m(\rho)$ is taken to be the melt temperature, determined from the Lindemann relation[2]. Since CH dissociates before melting, it is necessary to assume a value for the melt temperature at ambient pressure. The value used here, T_m=513.15 K, is the same as that used in LEOS-5400 for GDP.

The electronic excitation contribution to the free energy of LEOS-5112 comes from the Purgatorio atom-in-jellium calculations[119] for carbon and hydrogen. The Purgatorio cold curve is replaced by a Thomas-Fermi cold curve, and some data adjustment is done in the low tem-

perature region around equilibrium density to guarantee monotonicity in the pressure. These tables are then mixed using a constant-pressure, constant-temperature additive volume mix procedure. The resulting cold curve is then subtracted to yield the electron-thermal contribution used in the EOS. This includes the effects of shell structure, as well as relativistic effects at very high temperatures.

Figure 3 shows the specific heat at constant volume, C_V, for CH at a density of 3.15 g/cm^3. The black curve is the result of calculating $(\partial E/\partial T)_V$ directly from the DFT-MD (for $T \leq 10^6$ K) and PIMC (for $T > 10^6$ K) internal energies, by fitting a cubic spline to our 20 $E(T)$ points at this density and differentiating the smooth spline function. At the highest T, this asymptotes to 6.75 k_B/atom, which is the required value from equipartition, assuming complete ionization. There is a notable peak in this curve just above 10^6 K. The red curve shows C_V^{electron} from LEOS-5112, obtained as described above from the Kohn-Sham DFT average-atom Purgatorio model[119]. Though the peak is in a slightly different position than that seen in the black curve, this suggests that (a) the peak in C_V at $T = 10^6$ K arises from electronic ionization, and (b) this feature is modeled well by the comparatively simple Pugatorio treatment (which neglects, e.g., directional bonding). The temperature interval of the peak and related information presented in Refs. 24 and 29 suggest that its appearance results primarily from the ionization of the 1s electron shell of carbon. The green curve shows the black curve minus the red curve, which is an estimation of the ionic contribution to C_V, assuming the perfect additivity of electronic and ionic components together with the use of Purgatorio for the electronic piece. Note that it approaches the required value of 1.5 k_B/atom at high-T while rising slowly as T decreases, ultimately rising rapidly to a value of $\sim 3k_B$/atom at the lowest T (a value of $\sim$2.9 k_B/atom was predicted for CH$_{1.36}$ in Ref. 81). This rapid rise is reminiscent of behavior seen in DFT-MD calculations of pure carbon (see Fig. 9 of Ref. 19) where C_V was shown to drop quickly from $3k_B$/atom with increasing T over the range 2×10^4-8×10^4 K. Above a few times 10^4 K, the general behavior of the green curve is tracked rather well by the blue curve, which shows C_V^{ion} from LEOS-5112 at this density, given by the form in Eq. 1. With the exception of the small discrepancies at the lowest T of Fig. 3, the general agreement shown here provides validation for the manner in which the specific heat is modeled in LEOS-5112, indicating that at least the T-dependent part of E is treated reasonably well. This is noteworthy, for the work on pure carbon[19] demonstrated that the model of Eq. 1 was suspect even for T as high as 10^6 K. The behavior shown in Fig. 3 is reproduced in our other energy isochores as well.

While the temperature dependence of the internal energy of LEOS-5112 is therefore in quite good accord with that of our first-principles results throughout a wide range of density and temperature, the pressure of this
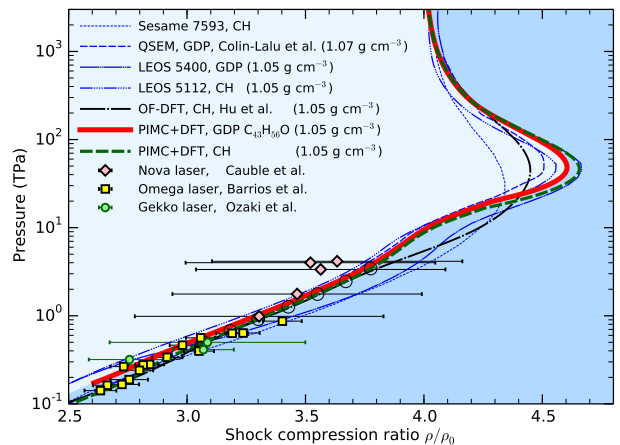

FIG. 5. Comparison of the shock Hugoniot curve of CH and GDP from first-principles calculations (PIMC and DFT-MD simulations or linear-mixing approximation in this work, OF-DFT and DFT-MD simulations in Ref. 94), EOS models (SESAME 7593[3], QSEM[96], LEOS 5400[117], LEOS 5112), and experiments[67,68,72,73]. Black circles are conditions chosen for examining the linear mixing approximation (see Sec. IV A).

model shows more significant discrepancies. Figure 4 shows isochores of P for four densities, $\rho = 2.1$, 3.15, 4.2, and 5.25 g/cm^3. At the lower-T, the pressures of the model are systematically too high; near-perfect agreement is only seen at much higher temperature, approaching the ideal gas limit. This suggests that the Grüneisen γ is too large in LEOS-5112, since this quantity does not enter the C_V discussed above. Still another possibility is that the cold curve of LEOS-5112 can benefit from slight modification, though our current inclination is to reinvestigate the combined Debye-Grüneisen and dissociation models pertaining to the ionic excitation contribution. Work to improve the EOS models of hydrocarbons such as CH using these first-principles simulations is ongoing. In the following Sec. III C, LEOS-5112 and LEOS-5400 are discussed again, in the context of predicted Hugoniot curves.

C. Shock compression

The locus of final states characterized by (E, P, V) accessible via a planar one-dimensional shock satisfy the Rankine-Hugoniot energy equation[120]

$$\mathcal{H}(T, \rho) = (E - E_0) + \frac{1}{2}(P + P_0)(V - V_0) = 0, \quad (2)$$

where (E_0, P_0, V_0) are the variables characterizing the initial (pre-shocked) state. This allows for the determination of the P-V-T Hugoniot curve with bi-variable spline fitting of the EOS data (E and P on a grid of T and V) in Sec. III A.

We thus obtain the principal Hugoniot curves of hydrocarbons[29] and represent that of CH (assuming

$\rho_0 = 1.05$ g/cm^3 and $T_0 = 300$ K) in a pressure-density plot (Fig. 5) together with experimental measurements at low pressures[67,68,72,73], OF-DFT simulations[94], and the Purgatorio-based LEOS 5112 (described above), QSEM[96], and the SESAME 7593[3] models. The DFT-MD predictions of the Hugoniot curve in this work and that of Ref. 94 agree well with experimental measurements, whereas SESAME 7593 deviates from the experimental data at 1-4 TPa. At 0.5 Gbar, we predict CH to reach a maximum compression (ρ/ρ_0) of 4.7, which is similar to that predicted by the LEOS 5400 model for GDP, and is higher than that of QSEM[96], LEOS 5112, and OF-DFT[94] by 2-5%; the SESAME 7593 model predicts the maximum compression to be smaller by 7.3% and the corresponding pressure about 17 megabar (Mbar) lower than our first-principles simulations. The compression maximum is originated from the 1s shell ionization of carbon. Since such temperature and pressure conditions correspond to the region at which PIMC works well and complexities such as electronic quantum effects, electronic correlation, and partial ionization are all essentially included in the quantum many-body framework, we expect the predictions in this work to be more reliable than those of semi-empirical models and OF-DFT. We note that the shock Hugoniot curve of CH obtained in this work is in remarkable agreement with that using a recent extended DFT method[121,122]. We look forward to accurate experiments in the Gbar regime which test these predictions.

Interestingly, our calculations and several other methods and models (Fig. 5) all have a shoulder along the Hugoniot curve at 4-fold compression. This corresponds to a pressure of 10 TPa and temperature of 5.7×10^5 K, according to the shock compression analysis of the first-principles EOS data in this work. The origin of this shoulder may be traced back to the start of ionization in the carbon 1s shell. Increasing amounts of carbon 1s electrons are excited at higher temperatures, as is shown in the $N(r)$ plot of Fig. 6. At 10^6 K, a noticeable amount of excitation can be seen. The ionization fraction of the carbon 1s shell grows considerably as temperature increases even further. Above 8×10^6 K, 1s ionization is complete and the system becomes an ideal plasma. Therefore the Hugoniot curves from different methods and models merge together and reach the ideal Fermi gas limit, which is consistent with the EOS comparisons and discussions in Sec. III A.

In order to better understand the differences between the Hugoniot curves from our simulations and the OF-DFT and DFT-MD study in Ref. 94, we compare the two components of the Hugoniot function in Fig. 7, i.e., the internal energy term $E - E_0$ and the pressure term $(P + P_0)(V - V_0)/2$, at two different temperatures. At 10^6 K, data in this work and those of Ref. 94 both rely on DFT-MD simulations, thus the energy and pressure values are similar. At 4×10^6 K, the OF-DFT pressure is slightly lower than that given by PIMC and the difference between them grows larger for higher densities, whereas the internal energy from OF-DFT is significantly lower
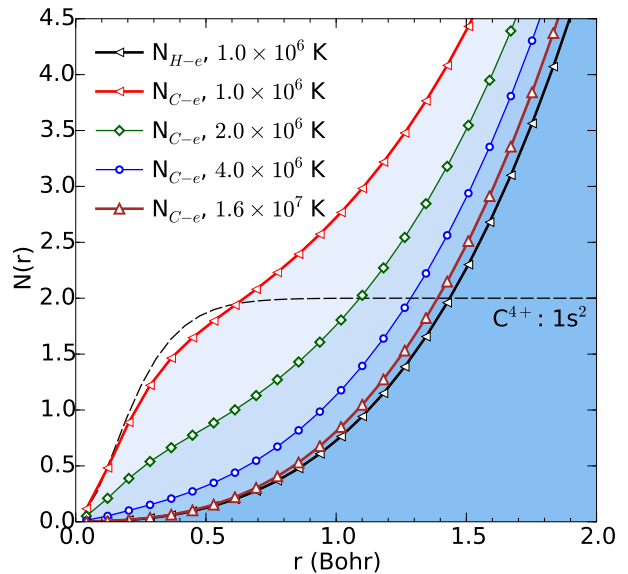

FIG. 6. The average number of electrons $N(r)$ around each carbon or hydrogen nucleus in CH at 3.15 g/cm^3 and a series of temperatures obtained from the PIMC simulations in this work. $N(r)$ is calculated via $N(r) = \left\langle \sum_{e,I} \theta(r - |\vec{r}_e - \vec{r}_I|) \right\rangle / N_I$, where the sum includes all electron-carbon ion or electron-hydrogen ion pairs and θ represents the Heaviside function. The corresponding profile of the C^{4+} ionization state, calculated with GAMESS, is shown for comparison.

than that of PIMC, resulting in lower densities along the Hugoniot curve. The differences between the Hugoniot curves from the two methods are similar to those found for Si[24]. These differences originate from the different treatments of electronic shell ionization effects in the two methods—PIMC is a many-body approach that accurately includes shell effects, while the OF-DFT approach makes use of what is essentially a Thomas-Fermi density functional which is not able to describe the shell structure accurately. Therefore, OF-DFT tends to smooth out ionization features near the compression maximum, leading to a single broad peak instead of the peak-shoulder (for CH) or double-peak (for Si) structures predicted by PIMC.

IV. DISCUSSION

A. Structure of the hydrocarbon fluid

In Ref. 29, we have shown that the isothermal isobaric linear mixing approximation works exceptionally well for stellar-core conditions. The validity of this approximation can be understood from analysis of the nuclear pair correlation functions, as is shown with the high-temperature (6.7×10^4 K) $g(r)$ profiles in Fig. S2 of Ref. 29 for CH and Fig. 8 for C$_2$H and CH$_2$. At these
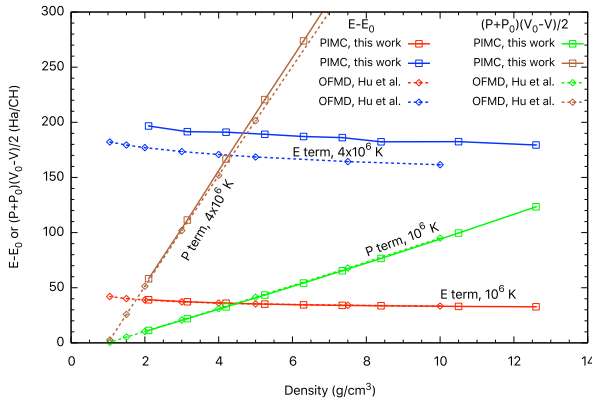
FIG. 7. Comparison of the energy and pressure components of the Hugoniot function of CH from this work (solid lines and squares) and from the OF-DFT model[94], dashed lines and diamonds) at two different temperatures. The initial state correspond to the ambient density of 1.05 g/cm^3. The densities at which the energy and pressure terms agree solve Eq. 2 and may be realized in experiments.
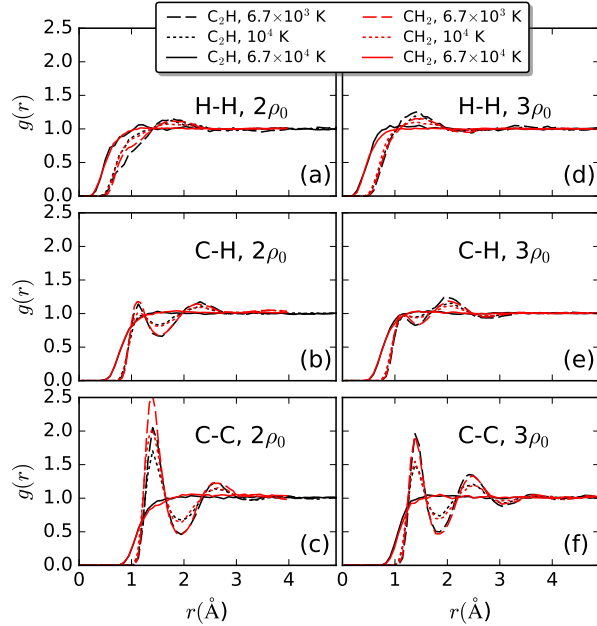

FIG. 8. Comparison of the nuclear pair correlation function obtained from DFT-MD for C_2H (dark) and CH_2 (red) at two different densities for every material and three temperatures. The reference density ρ_0 is 1.76 and 2.24 g/cm^3 for C_2H and CH_2, respectively.

extreme conditions, no C-H bonds exist (lifetime shorter than 4.4 fs, see Table I), and the non-existence of any peak structure in the pair-correlation function indicates that the system behaves similarly to an ideal yet partially ionized plasma. This explains the efficacy of the ideal linear mixing assumption manifested in the similarity between the Hugoniot curve as calculated from this
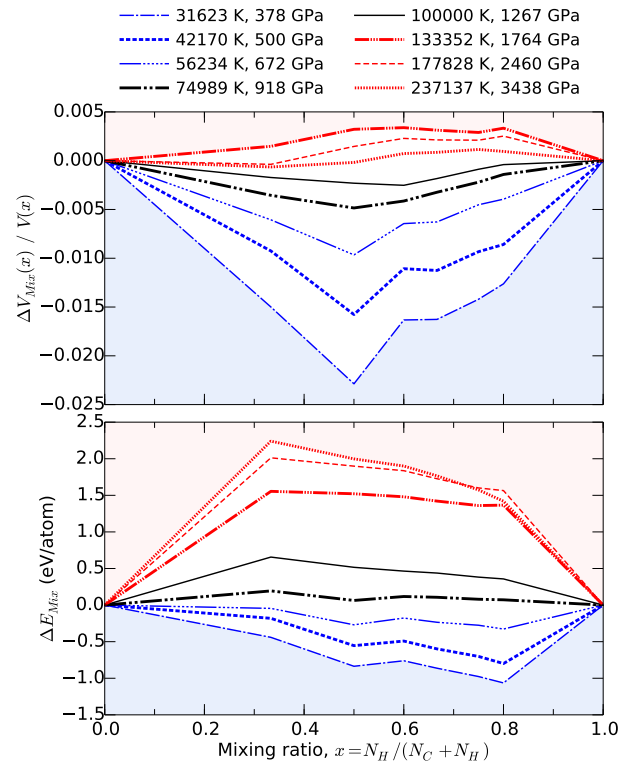

FIG. 9. The difference in energy (top) and volume (bottom) between bi-variable spline fitting of our first-principles EOS data of CH and the linear mixing approximation at a series of T, P conditions along the Hugoniot curve. The symbols are defined as $\Delta E_{Mix}(x) = E(x) - (1-x)E_C - xE_H$ and $\Delta V_{Mix}(x) = V(x) - (1-x)V_C - xV_H$.

approximation (using PIMC and DFT-MD EOS for the pure elements[19,103]), and the Hugoniot curve as calculated from our direct first-principles simulations of the mixtures in question[29].

Figure 9 compares the EOS of CH from interpolation of our first-principles data and that determined by the linear mixing approximation at a series of T, P conditions along the Hugoniot curve (Fig. 5). In comparison to interpolation of our first-principles EOS data, linear mixing of pure C and pure H overestimates the volume of CH by 2.3% at 3.2×10^4 K (378 GPa). The volume difference ΔV_{mix} decreases to within ±0.5% at $T > 5.6 \times 10^4$ K, which is consistent with the threshold temperature above which we see disappearance of peaks in the nuclear-pair correlation function $g(r)$ plots (Fig. 8). On the other hand, the energy of the linear mixture is higher than the first-principles value by 1.1 eV/atom at 3.2×10^4 K. The value of ΔE_{mix} decreases to 0-0.2 eV/atom at 7.5×10^4 K, and remains less than 2.5 eV/atom at higher temperatures. The fact that the energy of the linear mixture is smaller at the highest temperatures, while pressure is similar, explains why linear mixing predicts CH to be stiffer at the compression maximum than our direct first-principles predictions (Fig. 3 in Ref. 29).

TABLE I. Comparison of chemical bond lifetime τ in fs.

ρ (g/cm^3)	T (K)	P (Mbar)	$\tau_{\text{C-C}}$	$\tau_{\text{C-H}}$	$\tau_{\text{H-H}}$	$\tau_{\text{C-C-C}}$
2.10	6.7×10^3	0.44	89.62	16.68	4.60	44.12
2.10	1.0×10^4	0.61	48.77	11.36	4.00	23.92
3.15	6.7×10^3	1.76	69.72	12.63	4.18	35.67
3.15	1.0×10^4	2.04	43.13	10.19	3.80	21.72
3.15	2.0×10^4	2.89	25.63	7.58	3.15	12.93
3.15	5.0×10^4	5.55	14.63	5.06	2.28	7.55
3.15	6.7×10^4	7.19	12.44	4.34	2.06	6.58
3.15	1.3×10^5	13.4	9.50	3.30	1.60	4.88
3.15	2.0×10^5	22.1	7.47	2.68	1.32	3.85
3.15	5.1×10^5	60.9	4.70	1.66	0.88	2.47

At lower pressure and temperature, clear signatures of chemical bonds exist. Figure 8 compares the $g(r)$ profile of C_2H and CH_2 at two different densities ($2\times\rho_0$ and $3\times\rho_0$, with ρ_0= 1.76 and 2.24 g/cm^3 for C_2H and CH_2, respectively) and three different temperatures. For C-C $g(r)$ functions in Fig. 8(c) and (f), the results show clear peaks and structure at both temperatures of 6.7×10^3 and 10^4 K. These indicate the formation of carbon clusters. C-H bonds (Fig. 8(b) and (e)) also exist at these temperatures, characterized by the peak in $g(r)$ at $r\approx1.15$ Å. The C-H bonds are not very stable and are significantly weakened by thermal and compressional effects, as the differences in peak height show. We do not see any evidence of stable H-H bonds even at the the lowest temperature (6.7×10^3 K) that we considered (Fig. 8(a) and (d)), which is consistent with the analysis of other high pressure hydrogen-rich materials[123,124]. These peaks do not seem to be strongly dependent on the overall C:H ratio in the system and are consistent with findings in recent DFT-MD simulations[125] of CH_4.

A snapshot from the DFT-MD simulations of CH and its electronic density distribution at 3.15 g/cm^3 and 2×10^4 K is shown in Fig. 10. The disorder in the atomic positions is indicative of the plasma behavior, wherein ions participate in short-lived chemical bonding. Detailed structural analysis of the atomic bonding and lifetime at this condition (see Table I) indicates that C-C clusters and chains exist stably for the time scale of 10-100 fs, approximately one order of magnitude longer than H-H bonds. The lifetime of C-H bonds is slightly longer than 10 fs at $T < 10^4$ K and $\rho < 3.15$ g/cm^3, and is similar to (about two times) that of H-H bonds at higher T and P.

Changes in chemical bonding in hydrocarbons have been proposed to interpret experimental results along the Hugoniot curves. For example, Barrios et $al.$[73] tentatively attributed a slight softening that is observed for polystyrene at 2-4 Mbar to the decomposition of chemical bonds. Bond dissociation is also included in the SESAME EOS model for CH at 2-4 Mbar[3]. Our findings of dramatic decrease in the lifetimes of C-H bonds and changes in $g(r)$ at 0.4-4 Mbar are consistent with previous calculations[79,81,91,94]. However, our analysis shows that the decrease in bond lifetime is gradual, spaning
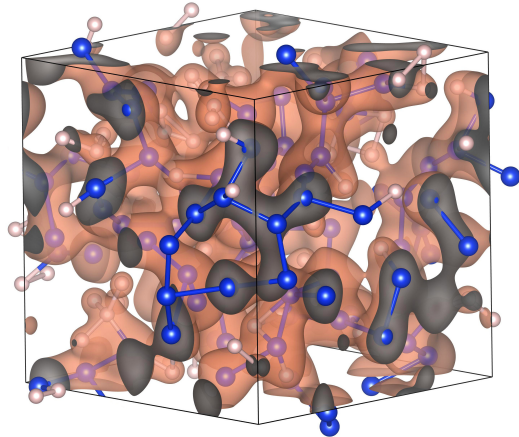

FIG. 10. A snapshot of the electron density profile of CH in the polymeric state[125] around thermodynamic equilibrium at 3.15 g/cm^3 and 2×10^4 K. The C and H atoms are represented by blue and pink spheres, respectively. Electron density which mitigates the bonding effects is illustrated by the light brown isosurface.
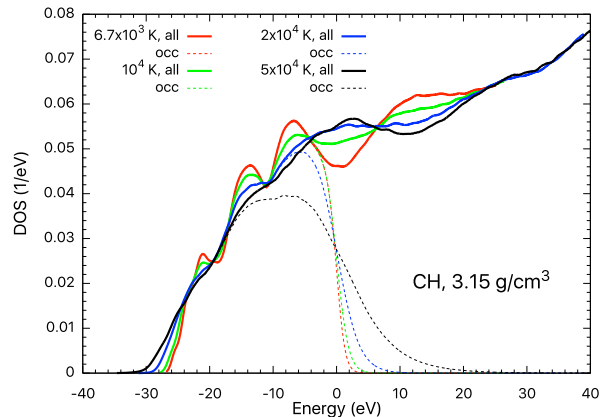

FIG. 11. Electronic density of states (DOS) of CH at a series of temperatures and 3.15 g/cm^3 based on Γ-point DFT simulations. The dashed curves denote the occupied states. The Fermi energies are aligned at E=0 eV. A pseudo-bandgap exists at 6.7×10^3 K. With increasing temperature, the gap is gradually filled. We have checked the results by using $2\times2\times2$ and $4\times4\times4$ Monkhorst-Pack k mesh[126], and found the same relation of the DOS curves.

a few Mbar and tens of thousands of Kelvin. This indicates that the dissociation of chemical bonds is continuous along the Hugoniot curve, instead of suddenly complete at certain T and P.

We also investigated the electronic density of states of CH at the same (ρ, T) conditions as in the $g(r)$ analyses (Fig. 8). We find a pseudo-bandgap exists at the valence band maximum at 6.7×10^3 K. This gap is partially filled, resulting in a more continuous transition between

the valence and the conduction bands, at 10^4 K, and is completely filled at 2×10^4 K (see Fig. 11). Closure of the gap indicates metalization of the system, which increases the electrical conductivity and reflectivity that can be observed in experiments. The corresponding pressure range (1.5-2.5 Mbar) is in accord with experimental findings[69,73] of optical reflectivity changes of CH samples. Note that band gap closure does not necessarily accompany complete chemical decomposition, because the changes in the lifetimes of the chemical bonds are gradual. It is therefore not appropriate to equate the origin of reflectivity change with chemical bond dissociation. We also do not see the changes in bonding to have an obvious effect on the shape of the Hugoniot curve.

B. Composition dependence of the Hugoniot curve of GDP

ICF experiments routinely use GDP as an ablator material; GDP is mostly hydrocarbon ($CH_{1.36}$) doped with small amounts of heavier elements, such as O or Ge. As has been shown in Sec. IV A and in Ref. 29, the linear mixing approximation is a reasonable way of estimating the EOS and shock compression of hydrocarbons. In this section, we apply this approximation to study the shock compression of GDP, compare with other EOS models, and investigate the effects of varying hydrogen and oxygen concentrations on the shock Hugoniot curve.

Figure 5 shows the Hugoniot curve of GDP ($C_{43}H_{56}O$), in comparison with those given by other models and that of CH. The initial density of GDP is set to 1.05 g/cm^3, as relevant to polystyrene and to the hydrocarbon materials used in recent laser shock experiments[77]. The initial energy E_0 is determined by approximating GDP as an ideal mixture of three polymers— PAMS (C_9H_{10}), polyethylene (C_2H_4) and polyvinylalcohol (C_2H_4O) —which allows for a higher flexibility in the composition of GDP. The energy of each polymer is determined as described in the supplementary material of Ref. 29. We determine the energy of diamond, isolated H_2 and O_2 molecules using DFT calculations and combine them with tabulated thermochemical data on the enthalpy of combustion[127,128] to estimate the energy of these polymers. As a proof of concept, we compare the energy of coronene $C_{24}H_{12}$ determined as a combination of PAMS and polyethylene to the thermochemical data and find very small difference (less than 15 mHa/carbon). Initial densities in Fig. 12 are determined in the ideal mixture approximation, using the density of PAMS (1.075 g/cm^3), polyethylene (0.95 g/cm^3) and polyvinylalcohol (1.19 g/cm^3).

Figure 5 shows the Hugoniot curve of GDP obtained from our first-principles EOS. It is slightly stiffer than that of CH at low pressures ($P < 5$ Mbar) and near the compression maximum. Similar trends are found in the results of the QSEM model[96]. For compression ratios between 3.3-4.3, a shoulder develops along the Hugoniot curve. The shoulder structure is also found along
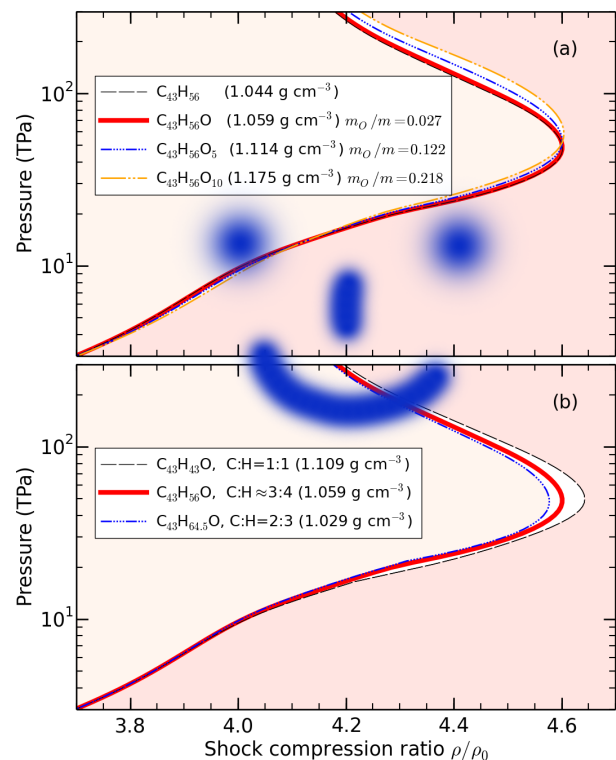

FIG. 12. Comparison of the effects of varying oxygen (a) and hydrogen (b) content on the shock Hugoniot curve of GDP.

the Hugoniot curve of LEOS 5400 GDP, which exhibits higher compressibility than that predicted by the first-principles calculations in this work. This may be traced to the start of ionization of the 1s electron shell of carbon, which leads to the shoulder, and the much lower Grüeneisen γ used in LEOS 5400 than in LEOS 5112 for compression ratios larger than 3.5, which causes the softer behavior predicted by LEOS 5400.

Considering that the chemical composition of GDP ablators varies[77,81,96,117], it is thus useful to compare the Hugoniot curves of GDP with different C:H ratios and oxygen contents. We consider three oxygen mass percentages of 2.7%, 12.2%, and 21.8%, and C:H ratios of 1:1, 1:1.33, and 1:1.5. A comparison of the Hugoniot curves is shown in Fig. 12. With the addition of oxygen, the pressure at the maximum compression increases, while the compression ratio does not show any observable change. The effect of oxygen can be understood from the fact that its 1s electrons are more strongly bound to the oxygen nuclei, which requires a higher temperature for ionization. Changes to the maximum compression ratio are insignificant within the range of oxygen content that we consider, because the carbon 1s electrons dominate over those of oxygen. Increasing the amount of hydrogen leads to a decrease by 0.1 in the compression maximum when the C:H ratio decreases from 1:1 to 1:1.5, as shown in Fig. 12(b). This is the same trend with composition that has been seen in Fig. 3 of Ref. 29. The pressure at

the compression maximum is not affected.

V. CONCLUSIONS

In this work, we presented the results of PIMC and DFT-MD simulations of a series of hydrocarbons. We obtained accurate internal energies and pressures from temperatures of 6.7×10^3 K to 1.3×10^8 K. PIMC and DFT-MD were shown to be consistent at 10^6 K, typically to within 1 Ha/carbon in energy and 3% in pressure. This cross-validates the use of both methods at the temperature of 10^6 K. We used these results to evaluate some of the detailed assumptions made in a recent EOS model for CH, LEOS-5112.

We investigated the principal Hugoniot curves using the obtained EOS data and found a maximum compression of 4.7, which is similar to that predicted by LEOS 5400 but larger than SESAME 7593 and OF-DFT predictions. We expect future experiments will test this prediction.

We demonstrated the validity of the linear mixing approximation in obtaining the EOS and shock Hugoniot curves of hydrocarbons. This can be explained by the unstable, short-lived C-H chemical bonds (lifetime $\tau < 4.4$ fs) for temperatures greater than 6.7×10^4 K. The nuclear-pair correlation function $g(r)$ of hydrocarbons resembles that of a simple atomic liquid at the higher temperatures we considered. At lower temperatures, $g(r)$ as well as bond lifetime analysis of hydrocarbon systems show the possible existence of stable C-C bonds with lifetimes of 10-100 fs, weak C-H bonds with lifetimes of 4-16 fs, and no signature of stable H-H bonds.

By applying the linear mixing approximation, we investigated the Hugoniot curves of GDP as a function of oxygen content and C:H ratios. We found that the compression maximum remains unchanged when varying the oxygen mass percentage between 0 and 21.8% while the pressure increases by about 0.1 Gbar. When the C:H ratio decreases from 1:1 to 1:1.5, the shock compression maximum decreases by 0.1 while the pressure, which is determined by the 1s ionization of carbon, does not change.

Our results provide a benchmark for future theoretical investigations of the EOS of hydrocarbons, and should be useful for informing on-going dynamic compression experiments aimed at reaching Gbar conditions.

VI. SUPPLEMENTARY MATERIAL

See the supplementary material for the tables of EOS data of C_2H, C_2H_3, CH_2, CH_3, and CH_4 considered in this study.

[1] W.-H. Tang, B.-B. Xu, X.-W. Ran, and Z.-H. Xu, Acta Physica Sinica **66**, 30505 (2017).

[2] R. M. More, K. H. Warren, D. A. Young, and G. B. Zimmerman, Phys. Fluids **31**, 3059 (1988).

[3] S. P. Lyon and J. D. Johnson, eds., *SESAME: The Los Alamos National Laboratory Equation of State Database* (Group T-1, Report No. LA-UR-92-3407, 1992).

[4] H. F. Wilson and B. Militzer, Phys. Rev. Lett. **104**, 121101 (2010).

[5] H. F. Wilson and B. Militzer, Phys. Rev. Lett. **108**, 111101 (2012).

[6] H. F. Wilson, M. L. Wong, and B. Militzer, Phys. Rev. Lett. **110**, 151102 (2013).

[7] S. M. Wahl and B. Militzer, Earth Planet. Sci. Lett. **410**, 25 (2015).

[8] S. Zhang, S. Cottaar, T. Liu, S. Stackhouse, and B. Militzer, Earth Planet. Sci. Lett. **434**, 264 (2016).

[9] F. Soubiran, B. Militzer, K. P. Driver, and S. Zhang, Phys. Plasmas **24**, 041401 (2017).

[10] M. A. Morales, J. M. McMahon, C. Pierleoni, and D. M. Ceperley, Phys. Rev. Lett. **110**, 065702 (2013).

[11] M. A. Morales, J. M. McMahon, C. Pierleoni, and D. M. Ceperley, Phys. Rev. B **87**, 184107 (2013).

[12] D. M. Ceperley, Rev. Mod. Phys. **67**, 279 (1995).

[13] D. M. Ceperley, in *Monte Carlo and Molecular Dynamics of Condensed Matter Systems*, Vol. 49, edited by K. Binder and G. Ciccotti (Editrice Compositori, Bologna, Italy, 1996) p. 443.

[14] C. Pierleoni, D. M. Ceperley, B. Bernu, and W. R. Magro, Phys. Rev. Lett. **73**, 2145 (1994).

[15] B. Militzer and D. M. Ceperley, Phys. Rev. E **63**, 066404 (2001).

[16] B. Militzer, Phys. Rev. B **79**, 155105 (2009).

[17] K. P. Driver and B. Militzer, Phys. Rev. Lett. **108**, 115502 (2012).

[18] B. Militzer and K. P. Driver, Phys. Rev. Lett. **115**, 176403 (2015).

[19] L. X. Benedict, K. P. Driver, S. Hamel, B. Militzer, T. Qi, A. A. Correa, A. Saul, and E. Schwegler, Phys. Rev. B **89**, 224109 (2014).

[20] K. P. Driver and B. Militzer, Phys. Rev. B **91**, 045103 (2015).

[21] B. Militzer and K. P. Driver, Phys. Rev. Lett. **115**, 176403 (2015).

[22] K. P. Driver, F. Soubiran, S. Zhang, and B. Militzer, J. Chem. Phys. **143**, 164507 (2015).

[23] K. P. Driver and B. Militzer, Phys. Rev. B **93**, 064101 (2016).

[24] S. X. Hu, B. Militzer, L. A. Collins, K. P. Driver, and J. D. Kress, Phys. Rev. B **94**, 094109 (2016).

[25] S. Zhang, K. P. Driver, F. Soubiran, and B. Militzer, High Energ. Dens. Phys. **21**, 16 (2016).

[26] K. P. Driver, F. Soubiran, S. Zhang, and B. Militzer, High Energ. Dens. Phys. **23**, 81 (2017).

[27] K. P. Driver and B. Militzer, Phys. Rev. E **95**, 043205 (2017).

[28] S. Zhang, K. P. Driver, F. Soubiran, and B. Militzer, J. Chem. Phys. **146**, 074505 (2017).

[29] S. Zhang, K. P. Driver, F. Soubiran, and B. Militzer, Phys. Rev. E **96**, 013204 (2017).

[30] C. Cazorla and J. Boronat, Rev. Mod. Phys. **89**, 035003 (2017).

[31] A. K. Rappé, C. J. Casewit, K. Colwell, W. Goddard Iii, and W. Skiff, J. Am. Chem. Soc. **114**, 10024 (1992).

[32] X. Gonze and C. Lee, Phys. Rev. B **55**, 10355 (1997).

[33] S. Baroni, S. De Gironcoli, A. Dal Corso, and P. Giannozzi, Rev. Mod. Phys. **73**, 515 (2001).

[34] W. M. Foulkes, L. Mitas, R. J. Needs, and G. Rajagopal, Rev. Mod. Phys. **73**, 33 (2001).

[35] F. Zhou, W. Nielson, Y. Xia, V. Ozoliņš, *et al.*, Phys. Rev. Lett. **113**, 185501 (2014).

[36] R. P. Feynman, (Addison-Wesley, Reading, MS, 1972).

[37] M. Jones and D. Ceperley, Phys. Rev. Lett. **76**, 4572 (1996).

[38] B. Militzer and R. L. Graham, J. Phys. Chem. Solids **67**, 2136 (2006).

[39] K.-d. Oh and P. Deymier, Phy. Rev. B **58**, 7577 (1998).

[40] C. Pierleoni and D. Ceperley, "The coupled electron-ion monte carlo method," in *Computer Simulations in Condensed Matter Systems: From Materials to Chemical Biology Volume 1*, edited by M. Ferrario, G. Ciccotti, and K. Binder (Springer Berlin Heidelberg, Berlin, Heidelberg, 2006) pp. 641–683.

[41] F. Graziani, M. P. Desjarlais, R. Redmer, and S. B. Trickey, *Frontiers and Challenges in Warm Dense Matter*, Vol. 96 (Springer Science & Business, 2014).

[42] J. M. McMahon, M. A. Morales, C. Pierleoni, and D. M. Ceperley, Rev. Mod. Phys. **84**, 1607 (2012).

[43] M. A. Morales, C. Pierleoni, E. Schwegler, and D. Ceperley, Proc. Natl. Acad. Sci. USA **107**, 12799 (2010).

[44] C. Pierleoni, M. A. Morales, G. Rillo, M. Holzmann, and D. M. Ceperley, Proc. Natl. Acad. Sci. USA **113**, 4953 (2016).

[45] E. Pollock and D. Ceperley, Phys. Rev. B **30**, 2555 (1984).

[46] B. Chen, I. Ivanov, M. L. Klein, and M. Parrinello, Phys. Rev. Letters **91**, 215503 (2003).

[47] J. A. Morrone and R. Car, Phys. Rev. Lett. **101**, 017801 (2008).

[48] M. Ceriotti, W. Fang, P. G. Kusalik, R. H. McKenzie, A. Michaelides, M. A. Morales, and T. E. Markland, Chem. Rev. **116**, 7529 (2016).

[49] M. Benoit, D. Marx, and M. Parrinello, Comput. Mater. Sci. **10**, 88 (1998).

[50] B. Pamuk, J. M. Soler, R. Ramírez, C. Herrero, P. Stephens, P. Allen, and M.-V. Fernández-Serra, Phys. Rev. Lett. **108**, 193003 (2012).

[51] R. Ramírez, C. P. Herrero, and E. R. Hernández, Phys. Rev. B **73**, 245202 (2006).

[52] R. O. Weht, J. Kohanoff, D. A. Estrin, and C. Chakravarty, The Journal of chemical physics **108**, 8848 (1998).

[53] A. W. Hauser, A. O. Mitrushchenkov, and M. P. de Lara-Castells, J. Phys. Chem. C **121**, 3807 (2017).

[54] R. Betti and O. Hurricane, Nature Phys. **12**, 435 (2016).

[55] N. Meezan, M. Edwards, O. Hurricane, P. Patel, D. Callahan, W. Hsing, R. Town, F. Albert, P. Amendt, L. B. Hopkins, *et al.*, Plasma Phys. Contr. Fusion **59**, 014021 (2016).

[56] V. Goncharov, S. Regan, E. Campbell, T. Sangster, P. Radha, J. Myatt, D. Froula, R. Betti, T. Boehly, J. Delettrez, *et al.*, Plasma Phys. Contr. Fusion **59**, 014008 (2016).

[57] T. Guillot, Annu. Rev. Earth Planet. Sci. **33**, 493 (2005).

[58] G. Wallerstein, I. Iben, P. Parker, A. M. Boesgaard, G. M. Hale, A. E. Champagne, C. A. Barnes, F. Käppeler, V. V. Smith, R. D. Hoffman, *et al.*, Rev. Mod. Phys. **69**, 995 (1997).

[59] G. Hauver and A. Melani, "Shock compression of plexiglas and polystyrene," Tech. Rep. (DTIC Document, 1964).

[60] I. Dudoladov, V. Rakitin, Y. N. Sutulov, and G. Telegin, J. Appl. Mech. Tech. Phys. **10**, 673 (1969).

[61] D. L. Lamberson, J. R. Asay, and A. H. Guenther, J. Appl. Phys. **43**, 976 (1972).

[62] S. P. Marsh, *LASL shock Hugoniot data*, Vol. 5 (Univ of California Press, 1980).

[63] W. J. Nellis, F. H. Ree, R. J. Trainor, A. C. Mitchell, and M. B. Boslough, J. Chem. Phys. **80**, 2789 (1984).

[64] R. Kodama, K. Tanaka, M. Nakai, K. Nishihara, T. Norimatsu, T. Yamanaka, and S. Nakai, Phys. Fluids B: Plasma Phys. **3**, 735 (1991).

[65] A. Bushman, I. Lomonosov, V. Fortov, K. Khishchenko, M. Zhernokletov, and Y. N. Sutulov, J. Exp. Theor. Phys. **82**, 895 (1996).

[66] M. Koenig, A. Benuzzi, B. Faral, J. Krishnan, J. Boudenne, T. Jalinaud, C. Rémond, A. Decoster, D. Batani, D. Beretta, *et al.*, Appl. Phys. Lett. **72**, 1033 (1998).

[67] R. Cauble, L. B. D. Silva, T. S. Perry, D. R. Bach, K. S. Budil, P. Celliers, G. W. Collins, A. Ng, J. T. W. Barbee, B. A. Hammel, N. C. Holmes, J. D. Kilkenny, R. J. Wallace, G. Chiu, and N. C. Woolsey, Phys. Plasmas **4**, 1857 (1997).

[68] R. Cauble, T. Perry, D. Bach, K. Budil, B. Hammel, G. Collins, D. Gold, J. Dunn, P. Celliers, L. Da Silva, *et al.*, Phys. Rev. Lett. **80**, 1248 (1998).

[69] M. Koenig, F. Philippe, A. Benuzzi-Mounaix, D. Batani, M. Tomasini, E. Henry, and T. Hall, Phys. Plasmas **10**, 3026 (2003).

[70] N. Ozaki, T. Ono, K. Takamatsu, K. Tanaka, M. Nakano, T. Kataoka, M. Yoshida, K. Wakabayashi, M. Nakai, K. Nagai, *et al.*, Phys. Plasmas **12**, 124503 (2005).

[71] S. Hu, V. Smalyuk, V. Goncharov, J. Knauer, P. Radha, I. Igumenshchev, J. Marozas, C. Stoeckl, B. Yaakobi, D. Shvarts, *et al.*, Phys. Rev. Lett. **100**, 185003 (2008).

[72] N. Ozaki, T. Sano, M. Ikoma, K. Shigemori, T. Kimura, K. Miyanishi, T. Vinci, F. Ree, H. Azechi, T. Endo, *et al.*, Phys. Plasmas **16**, 062702 (2009).

[73] M. Barrios, D. Hicks, T. Boehly, D. Fratanduono, J. Eggert, P. Celliers, G. Collins, and D. Meyerhofer, Phys. Plasmas **17**, 056307 (2010).

[74] H. Shu, S. Fu, X. Huang, G. Jia, H. Zhou, J. Wu, J. Ye, and Y. Gu, Chin. Opt. Lett. **8**, 1142 (2010).

[75] W. Shang, H. Wei, Z. Li, R. Yi, T. Zhu, T. Song, C. Huang, and J. Yang, Phys. Plasmas **20**, 102702 (2013).

[76] H. Shu, X. Huang, J. Ye, J. Wu, G. Jia, Z. Fang, Z. Xie, H. Zhou, and S. Fu, Eur. Phys. J. D **69**, 1 (2015).

[77] M. Barrios, T. Boehly, D. Hicks, D. Fratanduono, J. Eggert, G. Collins, and D. Meyerhofer, J. Appl. Phys. **111**, 093515 (2012).

[78] G. Huser, N. Ozaki, T. Sano, Y. Sakawa, K. Miyanishi, G. Salin, Y. Asaumi, M. Kita, Y. Kondo, K. Nakatsuka, *et al.*, Phys. Plasmas **20**, 122703 (2013).

[79] G. Huser, V. Recoules, N. Ozaki, T. Sano, Y. Sakawa, G. Salin, B. Albertazzi, K. Miyanishi, and R. Kodama, Phys. Rev. E **92**, 063108 (2015).

[80] A. S. Moore, S. Prisbrey, K. L. Baker, P. M. Celliers, J. Fry, T. R. Dittrich, K.-J. J. Wu, M. L. Kervin, M. E. Schoff, M. Farrell, *et al.*, High Energ. Dens. Phys. **20**, 23 (2016).

[81] S. Hamel, L. X. Benedict, P. M. Celliers, M. Barrios, T. Boehly, G. Collins, T. Döppner, J. Eggert, D. Farley, D. Hicks, *et al.*, Phys. Rev. B **86**, 094113 (2012).

[82] D. Kraus, D. A. Chapman, A. L. Kritcher, R. A. Baggott, B. Bachmann, G. W. Collins, S. H. Glenzer, J. A. Hawreliak, D. H. Kalantar, O. L. Landen, T. Ma, S. Le Pape, J. Nilsen, D. C. Swift, P. Neumayer, R. W. Falcone, D. O. Gericke, and T. Döppner, Phys. Rev. E **94**, 011202 (2016).

[83] D. C. Swift, J. A. Hawreliak, D. Braun, A. Kritcher, S. Glenzer, G. Collins, S. D. Rothman, D. Chapman, and S. Rose, AIP Conf. Proc. **1426**, 477 (2012).

[84] T. Döppner, A. Kritcher, D. Kraus, S. Glenzer, B. Bachmann, D. Chapman, G. Collins, R. Falcone, J. Hawreliak, O. Landen,

et al., J. Phys.: Conf. Ser. **500**, 192019 (2014).

[85] A. Kritcher, T. Döppner, D. Swift, J. Hawreliak, G. Collins, J. Nilsen, B. Bachmann, E. Dewald, D. Strozzi, S. Felker, *et al.*, High Energ. Dens. Phys. **10**, 27 (2014).

[86] A. L. Kritcher, T. Doeppner, D. Swift, J. Hawreliak, J. Nilsen, J. Hammer, B. Bachmann, G. Collins, O. Landen, C. Keane, S. Glenzer, S. Rothman, D. Chapman, D. Kraus, and R. Falcone, *J. Phys. Conf. Ser.*, **688**, 012055 (2016).

[87] J. Nilsen, B. Bachmann, G. Zimmerman, R. Hatarik, T. Döppner, D. Swift, J. Hawreliak, G. Collins, R. Falcone, S. Glenzer, *et al.*, High Energ. Dens. Phys. **21**, 20 (2016).

[88] R. Nora, W. Theobald, R. Betti, F. Marshall, D. Michel, W. Seka, B. Yaakobi, M. Lafon, C. Stoeckl, J. Delettrez, *et al.*, Phys. Rev. Lett. **114**, 045001 (2015).

[89] T. Doeppner and A. Kritcher, private communication.

[90] T. R. Mattsson, J. M. D. Lane, K. R. Cochrane, M. P. Desjarlais, A. P. Thompson, F. Pierce, and G. S. Grest, Phys. Rev. B **81**, 054103 (2010).

[91] C. Wang, X.-T. He, and P. Zhang, Phys. Plasmas **18**, 082707 (2011).

[92] F. Lambert and V. Recoules, Phys. Rev. E **86**, 026405 (2012).

[93] S. Hu, T. Boehly, L. Collins, *et al.*, Phys. Rev. E **89**, 063104 (2014).

[94] S. Hu, L. Collins, V. Goncharov, J. Kress, R. McCrory, S. Skupsky, *et al.*, Phys. Rev. E **92**, 043104 (2015).

[95] S. Hu, L. Collins, V. Goncharov, J. Kress, R. McCrory, and S. Skupsky, Phys. Plasmas **23**, 042704 (2016).

[96] P. Colin-Lalu, V. Recoules, G. Salin, T. Plisson, E. Brambrink, T. Vinci, R. Bolis, and G. Huser, Phys. Rev. E **94**, 023204 (2016).

[97] B. Militzer, Ph.D. Thesis, University of Illinois at Urbana-Champaign (2000).

[98] D. M. Ceperley, J. Stat. Phys. **63**, 1237 (1991).

[99] W. R. Magro, D. M. Ceperley, C. Pierleoni, and B. Bernu, Phys. Rev. Lett. **76**, 1240 (1996).

[100] B. Militzer, D. M. Ceperley, J. D. Kress, J. D. Johnson, L. A. Collins, and S. Mazevet, Phys. Rev. Lett. **87**, 275502 (2001).

[101] S. X. Hu, B. Militzer, V. N. Goncharov, and S. Skupsky, Phys. Rev. Lett. **104**, 235003 (2010).

[102] B. Militzer and D. M. Ceperley, Phys. Rev. Lett. **85**, 1890 (2000).

[103] S. X. Hu, B. Militzer, V. N. Goncharov, and S. Skupsky, Phys. Rev. B **84**, 224109 (2011).

[104] B. Militzer, W. Magro, and D. Ceperley, Contrib. Plasm. Phys. **39**, 151 (1999).

[105] B. Militzer, Phys. Rev. Lett. **97**, 175501 (2006).

[106] B. Militzer, J. Low Temp. Phys. **139**, 739 (2005).

[107] V. Natoli and D. M. Ceperley, J. Comp. Phys. **117**, 171 (1995).

[108] B. Militzer, Comput. Phys. Commun. **204**, 88 (2016).

[109] G. Kresse and J. Furthmüller, Phys. Rev. B **54**, 11169 (1996).

[110] P. E. Blöchl, O. Jepsen, and O. K. Andersen, Phys. Rev. B **49**, 16223 (1994).

[111] D. M. Ceperley and B. J. Alder, Phys. Rev. Lett. **45**, 566 (1980).

[112] J. P. Perdew and A. Zunger, Phys. Rev. B **23**, 5048 (1981).

[113] S. Nosé, J. Chem. Phys. **81**, 511 (1984).

[114] http://opium.sourceforge.net.

[115] A. Kramida, Yu. Ralchenko, J. Reader, and and NIST ASD Team, NIST Atomic Spectra Database (ver. 5.3), [Online]. Available: http://physics.nist.gov/asd [2017, August 3]. National Institute of Standards and Technology, Gaithersburg, MD. (2015).

[116] J. P. Perdew, K. Burke, and M. Ernzerhof, Phys. Rev. Lett. **77**, 3865 (1996).

[117] P. A. Sterne, L. X. Benedict, S. Hamel, A. A. Correa, J. L. Milovich, M. M. Marinak, P. M. Celliers, and D. E. Fratanduono, J. Phys. Conf. Ser. **717**, 012082 (2016).

[118] D. A. Young and E. M. Corey, J. App. Phys. **78**, 3748 (1995).

[119] B. Wilson, V. Sonnad, P. Sterne, and W. Isaacs, J. Quant. Spectrosc. Radiat. Transfer **99**, 658 (2006).

[120] M. A. Meyers, *Dynamic Behavior of Materials* (Wiley, New York, 1994).

[121] S. Zhang, H. Wang, W. Kang, P. Zhang, and X. T. He, Phys. Plasmas **23**, 042707 (2016).

[122] Private communication with Shen Zhang, Peking University.

[123] J. Vorberger, I. Tamblyn, B. Militzer, and S. A. Bonev, Phys. Rev. B **75**, 024206 (2007), 0609476.

[124] F. Soubiran and B. Militzer, Astrophys. J. **806**, 228 (2015).

[125] B. L. Sherman, H. F. Wilson, D. Weeraratne, and B. Militzer, Phys. Rev. B **86**, 224113 (2012).

[126] H. J. Monkhorst and J. D. Pack, Phys. Rev. B **13**, 5188 (1976).

[127] D. E. Roberts and R. S. Jessup, J. Res. Natl. Bur. Stnds. **46**, 11 (1951).

[128] R. N. Walters, S. M. Hackett, and R. E. Lyon, Fire Mater. **24**, 245 (2000).